

A close look at the well-known Seyfert galaxy: extended emission filaments in Mrk 6 [★]

Aleksandrina A. Smirnova ^{1†}, Alexei V. Moiseev ^{1,2‡}, and Sergei N. Dodonov ¹

¹ *Special Astrophysical Observatory, Russian Academy of Sciences, 369167 Nizhny Arkhyz, Karachaevo-Cherkesskaya Republic, Russia*

² *Space Research Institute, Russian Academy of Sciences, Profsoyuznaya ul. 84/32, Moscow 117997, Russia*

Accepted 2018 Month 00. Received 2018 Month 00; in original form 2018 Month 00

ABSTRACT

Using various techniques of optical observations at the 6-m Russian telescope (emission-line images, long-slit and 3D spectroscopy), we have studied large-scale morphology and kinematics of the ionized gas in the Seyfert galaxy Mrk 6. Having a significantly deeper images and spectra than those in previous works, we have not only mapped the ionized gas in the stellar disc but also found a system of faint filaments elongated in the NE direction up to a projected distance of 40 kpc ($4.3R_{25}$). Kinematics as well as an ionization state of the filament gas suggest the scenario that hard radiation of the active nucleus illuminated the matter accreted from outside and orbiting almost orthogonally to the Mrk 6 stellar disc. A possible source of gas accretion is still unknown, a deep image taken with the 1-m Byrakan Schmidt telescope does not show any stellar counterparts at the level of 27–28 mag arcsec^{−2}.

Key words: galaxies: individual: Mrk 6 – galaxies: interactions – galaxies: Seyfert – galaxies: ISM – ISM: kinematics and dynamics.

1 INTRODUCTION

The central engines of active galactic nuclei (AGN) have a significant impact on the ambient interstellar medium via relativistic jets, gas outflow, and collimated hard ionizing radiation. In some cases, Extended Emission-Line Regions (EELRs) are observed at as far as tens kiloparsecs. In radio-quiet objects including local Seyfert galaxies, the jet-cloud interaction occurs only in the central several kiloparsecs, while the rest parts of an EELR ionized by the AGN radiation appear in a broad cone. Recent works used EELRs to probe the history of an AGN radiative output across the light-travel times to the external gaseous clouds (‘a quasar light echo’, Lintott et al. 2009; Keel et al. 2012) that is also called the ‘AGN archeology’ (Morganti 2017). The other aspect of the EELR study related with the AGN illumination of gas outside the main galaxy disc: off-plane tidal debris (Keel et al. 2015) or even cosmic web filaments (Cantalupo et al. 2014). Therefore, the study of EELRs highlights the processes of baryon mass assembly by galaxies

with significantly higher angular resolution than that in radio observations of neutral H I. In this Letter, we described the system of extended filaments around the Mrk 6 AGN serendipitously discovered in the scanning Fabry-Perot Interferometer (FPI) observations at the 6-m telescope of the Special Astrophysical Observatory of the Russian Academy of Sciences (SAO RAS).

Mrk 6 is a well-known S0 galaxy identified as an intermediate Seyfert through the optical spectroscopy by Osterbrock & Koski (1976). It has a strongly variable continuum and broad Balmer lines (Khachikian & Weedman 1971; Eracleous & Halpern 1993; Doroshenko et al. 2012, and references therein) extensively studied spectroscopically, the mass of the central black hole is about $1.5 \times 10^8 M_{\odot}$ according to the spectropolarimetry by Afanasiev et al. (2014). Mrk 6 reveals a complex structure of radio emission: a compact radio core and elongated multicomponent radio structures which resemble jet elements and/or hot spots. It is also one of Seyfert galaxies that have radio emission on both small and large (~ 15 kpc in diameter) scales (Kukula et al. 1996; Kharb et al. 2014), its complex radio emission is argued to have been possibly originated by an episodically powered precessing jet (Kharb et al. 2006). HST images also show jet-like emission feature extending at ~ 200 pc, which is co-spatial with a radio jet seen in the 6-cm radio data by Capetti et al. (1995). The ground-based imaging and spectral observations revealed a large ($r \approx 22$ kpc) EELR with a multi-

[★] Based on observations obtained with the 6-m telescope of the Special Astrophysical Observatory of the Russian Academy of Sciences carried out with the financial support of the Ministry of Education and Science of the Russian Federation (agreement No. 14.619.21.0004, project ID RFMEFI61914X0004).

[†] E-mail: ssmirnova@gmail.com

[‡] E-mail: moisav@gmail.com

Table 1. Log of observations at the SAO RAS 6-m telescope

Date	Instrument/mode	Exp. time, s	Sp. range, Å	Sp. resol. (FWHM), Å	Seeing, arcsec
22/23 Feb 2006	SCORPIO/FPI	32×300	H α	2.6	1.8–2.2
16/17 Dec 2014	SCORPIO-2/IM	7×600	H α_{on}		1.6
		7×180	H α_{off}		1.6
05/06 Mar 2014	SCORPIO-2/IM	5×300	[OIII] $_{on}$		2.6
		5×300	[OIII] $_{off}$		2.6
01/02 Apr 2016	SCORPIO-2/IM	5×120	<i>g</i> -sdss		1.8
		4×90	<i>r</i> -sdss		1.6
		5×150	<i>i</i> -sdss		1.7
05/06 Mar 2014	SCORPIO-2/LS PA=144°	2×900	3650–7230	4.5	2.4
	SCORPIO-2/LS PA=226°	2×900	3650–7230	4.5	2.8
02/03 Dec 2000	MPFS	3×1200	3750–6370	8.0	2.0

component structure of the emission-line profiles in the circumnuclear ($r < 3$ kpc) region, whereas the gas emission outside demonstrates a single kinematic component with a low velocity dispersion (Meaburn, Whitehead & Pedlar 1989). Afanasiev & Silchenko (1991) used optical spectroscopic data taken in five different long-slit positions together with integral-field observations to reconstruct the ionized gas kinematics of EELR, the observed picture was very complex: the authors decided that the inner region has a possible opposite rotation with significant outflow motions, whereas the other part of the gaseous disc is inclined by 40° to the galaxy’s line-of-sight. These controversial kinematics was the reason to select this target for our 3D spectroscopic observations. We adopted the distance to the galaxy as 80.6 Mpc (Kharb et al. 2006) with the scale of 0.39 kpc per arcsec.

2 OBSERVATIONS AND DATA REDUCTION

Observations were carried out at the prime focus of the 6-m SAO RAS telescope in different modes of the SCORPIO (Afanasiev & Moiseev 2005) and SCORPIO-2 (Afanasiev & Moiseev 2011) focal reducers in 2006–2016. Also, we used the 6-m telescope archival data obtained with the integral-field Multi-Pupil Field Spectrograph (MPFS, Afanasiev, Dodonov & Moiseev 2001). The log of observations and parameters of the used instruments are listed in Table 1. The main steps of data reduction and references to the software are presented in our previous papers (Smirnova & Moiseev 2010; Egorov et al. 2018). SCORPIO/SCOPRIO-2 provided 6.1-arcmin field of view (and the same length of the long slit with the 1-arcsec width for spectroscopy) with the 0.35-arcsec pixel scale. The scanning FPI mapped the spectral region around the redshifted H α emission line in 32 spectral channels. We made additional binning of these data to reach a higher signal-to-noise (S/N) ratio in the resulting data cube with 0.7 arcsec per pixel. The MPFS data cube covered the larger spectral range in the 16×16 arcsec² field-of-view centered at the nucleus, the spatial scale was 1 arcsec.

The narrow-band images were taken through filters centered on the redshifted H α and [O III] λ 5007 emission lines and the nearest continuum. The corresponding filters are marked with the indexes ‘on’ and ‘off’ in Table 1. The FWHM filters were 79Å for the H α_{off} filter and 15–33Å in other cases. Calibration of these narrow-band images as

well as the SCORPIO-2 and MPFS spectra into the absolute energetic flux units was performed using spectrophotometric standard stars observed in the same nights as Mrk 6. In order to convert the broad-band images in the SDSS *gri* filters into the scale of magnitudes, we used the photometric catalogue of the Pan-STARRS1 field stars (Magnier et al. 2016).

Also, deep images of the $\sim 1^\circ$ field centered at Mrk 6 were obtained at the 1-m Schmidt telescope (Byurakan Astrophysical Observatory (BAO) of the National Academy of Sciences of Armenia) in the *gri* SDSS filters in Nov 5–6, 2016. The total exposure was 55 min in each filter with a typical seeing of ~ 3 arcsec with the 0.87-arcsec pixel scale. The description of this camera and the data reduction process were presented by Dodonov et al. (2017). Calibration of the images into magnitudes was performed in the same manner as for the SCORPIO-2 broad-band images.

3 MORPHOLOGY AND GAS KINEMATICS

Figure 1 shows the composite *gri* SCORPIO-2 image of the galaxy that is significantly deeper than the broad-band images published previously. The 1σ noise level in background pixels corresponds to surface brightnesses of 27.7, 27.4, and 27.2 mag arcsec^{−2} in the *g*, *r*, and *i* filters, respectively. This image does not reveal any considerable peculiarities (tidal features or asymmetric structures) in the distribution of the stellar component. The only exception is low-contrast arches or a pseudo ring at the distances $r \approx 60$ arcsec near the galaxy’s major axis. However, the observed morphology changes dramatically in the ionized-gas emission lines. The 6-m telescope narrow-band images and FPI maps clearly demonstrate that the EELR known early and extending at $r = 13$ –22 kpc (Meaburn et al. 1989; Kukula et al. 1996) is only an inner part of a giant system of knots and diffuse filaments. The filaments were detected up to a surface brightness level of $\sim 5 \cdot 10^{-18}$ erg s^{−1} arcsec² in the H α emission line and $\sim 1 \cdot 10^{-17}$ erg s^{−1} arcsec² in [O III] that is six times fainter than those in the Meaburn et al. (1989) images. The most extended filaments elongate in the NE direction at the projected distance $r = 102$ arcsec (~ 40 kpc) that corresponds to $4.3R_{25}$ ($R_{25} = 24$ arcsec according to the NED database).

The bottom panels in Fig. 1 show the maps derived from the one-component Voigt fitting of the H α spectra in

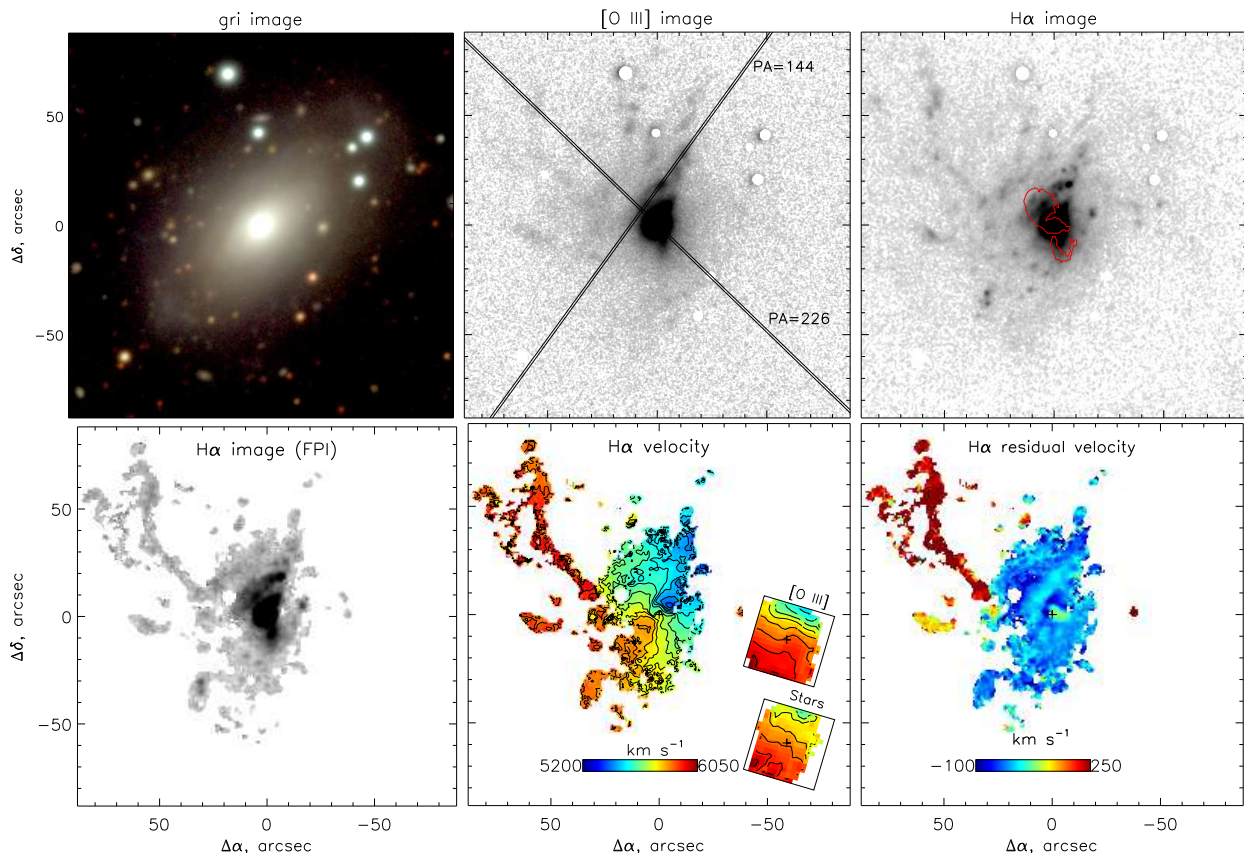


Figure 1. Mrk 6 data obtained at the 6-m telescope. Direct images are in the top row: the *gri* composite image (left-hand); the [O III] emission line image with marked slit positions (middle); the H α image (right-hand), the red contours mark the external border of the radio structure on 20 cm (Kharb et al. 2006). 3D spectroscopic data are in the bottom row: the map of the H α emission obtained from the lines fitting the FPI data cube (left-hand); the line-of-sight velocities in H α according to FPI observations together with the circumnuclear (16×16 arcsec²) MPFS velocity fields of stars and the ionized gas in [O III] (middle); the residual H α velocities after subtraction of the disc circular rotation model (right-hand).

the FPI data cube. The distribution of emission structures in the FPI H α monochromatic map agrees very well with the narrow-band direct image if some difference in the detection limit are taken into account.

The inner part of the H α velocity field ($r < 60$ arcsec) has a pattern typical of dominating circular rotation. To describe the gas kinematics quantitatively, we fitted the velocity field with a classical ‘tilted-ring’ model using the technique described in Smirnova & Moiseev (2010); Moiseev (2014, and references therein). We kept the disc inclination along the radius as $i = 57^\circ$ according to our estimation of the outer *g*- and *r*-band isophotes.

The radial changes of the rotation velocity V_{rot} and major kinematic axis PA_{kin} are shown in Fig. 2. The H α velocity field might be divided into two components: (i) the galaxy disc and (ii) the external filaments. In the inner gaseous disc, the radial variation of PA_{kin} around its mean value of $133 \pm 3^\circ$ are negligible up to $r \approx 60$ arcsec (22 kpc) that agrees very well with the position angle of the stellar continuum isophotes. The velocity field of the stellar component in the circumnuclear ($r < 10$ arcsec) region derived from the MPFS data cube using the cross-correlation technique (as described in Smirnova & Moiseev 2010) also has the same PA_{kin} . Therefore, the gaseous disc

co-rotates with the stellar one. The typical value of residual velocities after subtraction of the tilted-ring model is about ± 30 km s⁻¹, while they reach an amplitude of 85–120 km s⁻¹ in several regions near the nucleus at $r < 9$ arcsec. These non-circular motions seem to be related with the AGN outflow and jet-cloud interaction and located near the edges of the radio structure as presented in Kharb et al. (2006). Additional evidence of the AGN influence on the surrounding-gas kinematics is provided by significant variations of PA_{kin} estimated in the high-excited [O III] emission lines in our MPFS data (the MPFS maps are shown in Fig. 1 as insets in the panel with the H α velocity field). Our spatial resolution is insufficient for a detailed study of gas properties in these regions which were recently mapped with the subarcsecond integral-field observations by Freitas et al. (2018). The authors also stressed the distinct rotation pattern in the [O III] and H α velocity fields related to gas compression by the jet. The multicomponent structure of narrow lines in this region was also mentioned by Meaburn et al. (1989) and Afanasiev & Silchenko (1991).

The kinematics of the external gaseous filaments NE to the nucleus is fully decoupled from the disc circular rotation. Indeed, the map of residuals in Fig. 1 shows that the observed line-of-sight velocities exceed the extrapolation of

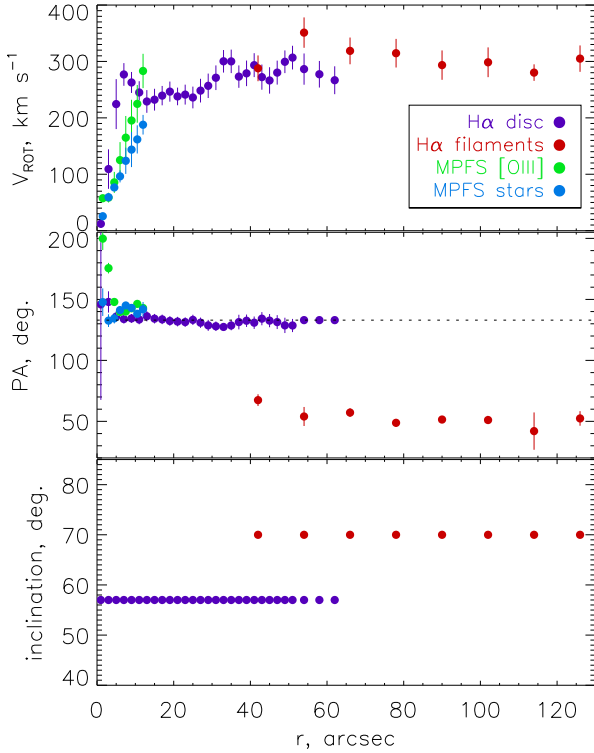


Figure 2. Radial variations of the tilted-ring model parameters: the circular rotation velocity (top), the position angle (middle) and the accepted inclination (bottom). The dashed line marks the PA of the galaxy’s stellar disc.

the circular rotation model by $100\text{--}300\text{ km s}^{-1}$. It is interesting that this peculiar kinematics also can be described in a ‘tilted-ring’ model of rotation, if we assume the same systemic velocity as that for the galaxy’s disc and inclinations of about 70° . The model solution for this case seems to be very reasonable (the red symbols in Fig. 2): a flat rotation curve with the same amplitude as that for the Mrk 6 disc up to $r = 125$ arcsec and a relatively small variation $PA_{kin} \approx 50^\circ$ in the agreement with the observed extension of the filaments. In this case, the external gas rotates around Mrk 6 in the polar plane almost orthogonally to the galaxy’s stellar disc.

4 GAS EXCITATION

In order to study a gas ionization origin, we made two cross-sections with SCORPIO-2 in the long-slit spectroscopy mode: in $PA = 144^\circ$ (along the brightest part of the [O III] structure N to the nucleus near the position already studied spectroscopically in Meaburn et al. 1989) and along $PA = 226^\circ$ (through the nucleus and the brightest part of the distant filament). The example of the latter spectrum is shown in Fig. 3. We were able to detect the brightest emission lines ($H\alpha$, $H\beta$, [N II], and [O III]) in the distant emission knot at $r \approx 77$ arcsec. Figure 4 presents the emission-line ratios for the [N II] $\lambda 6583/H\alpha$ and [O III] $\lambda 5007/H\beta$ diagram (the BPT diagram after Baldwin, Phillips & Terlevich 1981) based on the Gaussian fitting of the emission lines along both slits with the 2.8-arcsec sampling. Only the regions

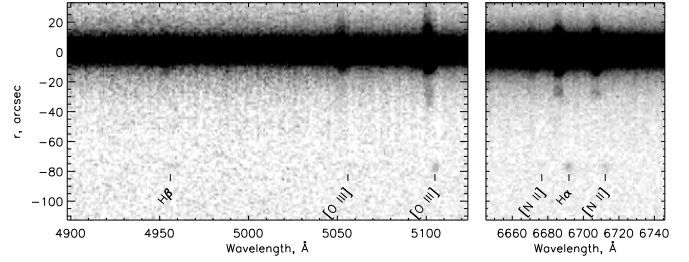


Figure 3. Mrk 6 spectrum along $PA = 226^\circ$: fragments of the 2D spectrum around the $H\beta$ + [O III] $\lambda\lambda 4959, 5007$ and $H\alpha$ + [N II] $\lambda\lambda 6548, 6583$ regions binned to a scale of 1.4 arcsec along the slit.

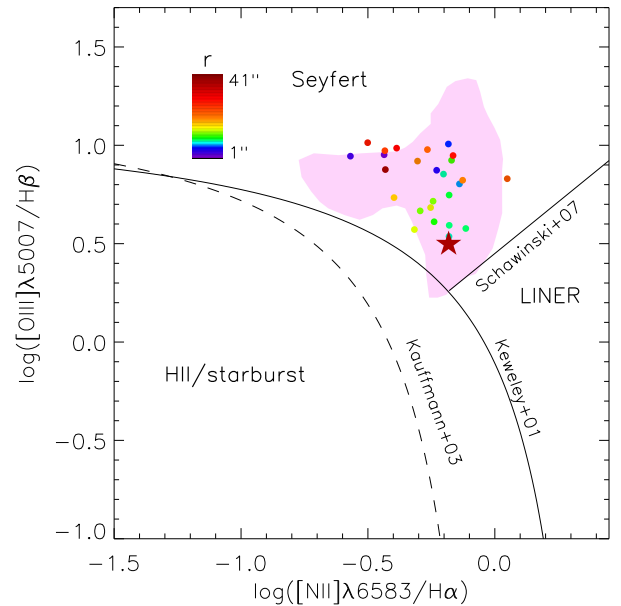


Figure 4. BPT diagram for the spectra along $PA = 144^\circ$ and 226° , different colours correspond to radial distances along the slit according to the scale box. The red star marks emission-line fitting results for the spectrum shown in Fig. 3 integrated over $r = -82.. -72$ arcsec. The division lines between star-forming galaxies, Seyfert and LINER nucleus are taken from Kauffmann et al. (2003), Kewley et al. (2001), and Schawinski et al. (2007). The violet filled regions mark the envelope of the main part of points in the 3×5 arcsec central field according to Freitas et al. (2018).

with $S/N > 2$ in all the lines were included in this plot. All the measurements in the galactic disc region ($r < 40$ arcsec) including the above-mentioned emission knot are located in the Seyfert region of the BPT diagram implying that even at these large distances, the AGN radiation is dominated in gas excitation similar to the Fischer et al. (2017) data for the inner part of the EELR.

The ratio of the narrow-band emission-line images reveals several compact emission knots in the galactic disc ($r = 20 - 50$ arcsec) with domination of the Balmer line emission: $[O III] \lambda 5007 / H\alpha \leq 0.3$ that corresponds to $[O III] \lambda 5007 / H\beta \leq 1$. However, SCORPIO-2 slits did not cross these HII regions.

5 DISCUSSION

Our new data reveal a complex structure of the EELR in Mrk 6 consisting of a gaseous disc co-rotating with the galaxy's stellar disc and off-plane ionizing filaments extended to a projected distance of 40 kpc. The BPT diagram suggests that the AGN hard radiation is a dominant source of gas ionization. However, the corresponding line ratios lie near the separation borders of Syfert/LINER/Starbursts, therefore, the ionization balance should be checked. Based on the technique and assumptions described in details by Keel et al. (2017) ('case B' recombination, similarity of the densest gaseous clouds at various radii r), we can write the ratio of the required emission rate of ionizing photons (Q_{ion}) needed to produce the observed $H\alpha$ surface brightness F to the same rate powered by the observed-epoch nuclear $H\alpha$ flux (F_{nuc}) as: $a_{ion} = Q_{ion}/Q_{nuc} = 4\pi r^2 F/F_{nuc}$, where r is in the same units as a square for F (px, arcsec, etc.). Applying this relation to our narrow-band $H\alpha$ image with $F_{nuc} = 5.9 \cdot 10^{-13} \text{ erg s}^{-1} \text{ cm}^{-2}$ estimated in the 6-arcsec diameter aperture, we obtained $a_{ion} < 1-3$ in all the radii. The real value of a_{ion} might be even smaller, because we significantly underestimate Q_{nuc} in this calculation neglecting the dust absorption and circumnuclear gaseous clouds covering factor. Therefore, we can conclude that the present AGN radiation is enough for ionization of the whole EELR.

Formation of the extended filaments via the nuclear activity (AGN outflow, star burst wind, or jet-cloud interaction) contradicts its observed properties: (i) the gas is dynamically cold according to the FPI data on the velocity dispersion in the filaments which is similar to those in the unperturbed regions in the disc ($\sigma < 30 - 50 \text{ km s}^{-1}$); (ii) the radio jet does not extend to the corresponding distances; (iii) we do not see a counter-structure expected for a symmetric outflow; (iv) the spatial scale of a possible outflow is typical of a more powerful active nucleus (radio-loud QSO).

An alternative supposition is an external matter orbiting orthogonally to the stellar disc according to our analysis of the $H\alpha$ velocity field. In this case, the origin of the NE filaments in Mrk 6 is similar to that in gaseous clouds in tidal tails and debris caught in the ionization cone of the AGN, e.g., the sample compiled by Keel et al. (2012). The kinematics of these structures (the domination of rotation, a small velocity dispersion) according to Keel et al. (2015) is in agreement with the picture observed in Mrk 6, as well as with spatial scales. For instance, the EELR in NGC 5972 is detected at $r \approx 50$ kpc together with the stellar tail (Keel et al. 2012).

With the aim to find possible stellar counterparts of the gaseous structure, we performed deep imaging observation of the Mrk 6 environment at the 1-m Schmidt telescope of BAO (Section 2) having a very low level of the scattered light as compared to the 6-m telescope data essential for detecting faint structures. The reached 1σ noise level corresponds to surface brightnesses in the g, r, i filters: 28.1, 27.5, and 26.9 mag arcsec $^{-2}$, respectively. The deepest g -band image shown in Fig. 5 reveals a large-scale filamentary system of the Milky Way cirrus elongated mostly in the N-S direction with a typical brightness of ~ 26.5 mag arcsec $^{-2}$ seen in all the filters. However, we do not see any structures which might be interpreted as tidal stellar streams related to the accreted gas. Only one possible

source of accretion has appeared in our deep images – the IC 451 galaxy which is similar in luminosity to Mrk 6 at a projected distance of 98 kpc. Moreover, the galaxy's disc has an asymmetric one-armed structure (the inset in Fig. 5) that could be related to a tidal interaction in the past; the Mrk 6 gaseous filaments are located exactly along the line between these galaxies. Can we consider the kinematically decoupled gaseous system in Mrk 6 as the first stage of formation of a gaseous polar ring in agreement with a popular accretion scenario (Reshetnikov & Sotnikova 1997; Bournaud & Combes 2003)? We have only one strong argument against this hypothesis. The IC 451 systemic velocity equal to $5123 \pm 53 \text{ km s}^{-1}$ (according to NED) is 500 km s^{-1} smaller than that in Mrk 6; it is too high for a gravitationally bound pair of galaxies. Even if we observe the first passage of IC 451 near Mrk 6, it is difficult to understand how the accreted gas dramatically changed its own angular momentum to reach observed line-of-sight velocities of $\sim 6000 \text{ km s}^{-1}$ that by 700 km s^{-1} differs from those of IC 451.

The observed difference of the line-of-sight velocities in the system Mrk 6–filaments gas–IC451 also rules out the hypothesis that the elongation of the most extended filaments in the NE direction is caused by a recent collision between the galaxies. Indeed, one of the best illustrations of such interaction appears in the Virgo cluster: the gas stripping from the spiral galaxy NGC 4438 after its collision with the M 86 elliptical galaxy. The result is a system of $H\alpha$ filaments connecting both companions of the pair (Kenney et al. 2008). However, in this case a smooth gradient of the line-of-sight gas velocities is expected, i.e., the value of filament velocities should be between systemic velocities of both companions, as it is observed in M86/NGC 4438 according to Kenney et al. (2008). While this predicted picture significantly contradicts the velocity distribution in the Mrk 6 environment. Moreover, as we already mentioned in Sec. 3, the disc of Mrk 6 has a very regular symmetric structure that is inconsistent with a recent flyby interaction with a massive galaxy (see Mapelli et al. 2008, as an example of simulations).

Another way of formation of a one-sided 'tail' of warm emitted gas is a ram-pressure stripping caused by the hot intergalactic medium in clusters or even in groups. The Seyfert galaxy NGC 4388 is a well-known example of such filaments (Yoshida et al. 2004, and references therein). However, we have no evidence of a hot X ray halo around/near Mrk 6 in the literature. The published *Chandra* and *XMM-Newton* data reveal the hot gas only in the central bubbles ($r < 8$ kpc) related to the AGN-driven outflow (Mingo et al. 2011).

Therefore, all the available observed data are consistent with a supposition that anisotropic radiation of the Seyfert nucleus collimated in a broad cone allows us to see a part of an off-plane gaseous structure orbiting around Mrk 6. We restored its kinematics and the ionization state, while a possible source of gas accretion is ambiguous. We hope that new deep HI radio observations of this field will make it possible to reveal a clear picture of the gaseous environment and accretion processes around this well-known AGN.

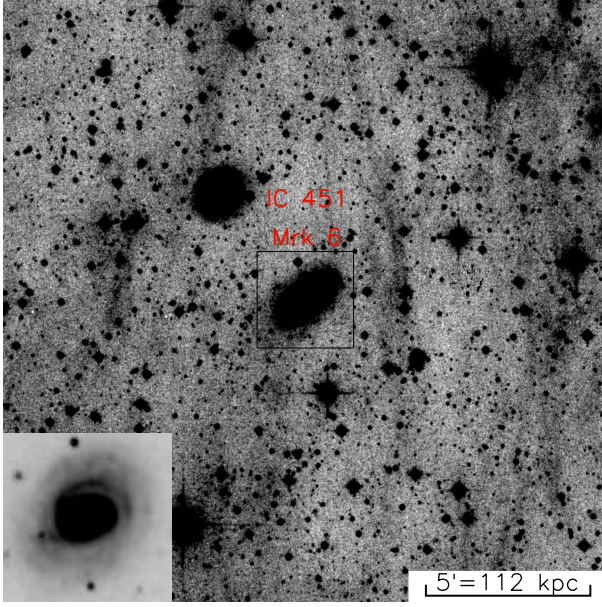


Figure 5. Deep image of the Mrk 6 environment in the g -band obtained with the 1-m Schmidt telescope of BAO. The square marks the field shown in Fig. 1. The inset shows the zoomed 1/5 field centered at IC 451.

6 ACKNOWLEDGEMENTS

The study was supported by the Russian Science Foundation, project no. 17-12-01335. We wish to thank an anonymous reviewer for constructive comments which have helped us to improve the paper. This research has made use of the NASA/IPAC Extragalactic Database (NED) which is operated by the Jet Propulsion Laboratory, California Institute of Technology, under contract with the National Aeronautics and Space Administration.

References

Afanasiev V. L., Moiseev A. V., 2005, *Astronomy Letters*, **31**, 194
 Afanasiev V. L., Moiseev A. V., 2011, *Baltic Astronomy*, **20**, 363
 Afanasiev V. L., Silchenko O. K., 1991, *Astrofizicheskie Issledovaniia*, **33**, 132
 Afanasiev V. L., Dodonov S. N., Moiseev A. V., 2001, in Ossipkov L. P., Nikiforov I. I., eds, *Stellar Dynamics: from Classic to Modern*. p. 103
 Afanasiev V. L., Popović L. Č., Shapovalova A. I., Borisov N. V., Ilić D., 2014, *MNRAS*, **440**, 519
 Baldwin J. A., Phillips M. M., Terlevich R., 1981, *PASP*, **93**, 5
 Bournaud F., Combes F., 2003, *A&A*, **401**, 817
 Cantalupo S., Arrigoni-Battaia F., Prochaska J. X., Hennawi J. F., Madau P., 2014, *Nature*, **506**, 63
 Capetti A., Axon D. J., Kukula M., Macchetto F., Pedlar A., Sparks W. B., Boksenberg A., 1995, *ApJ*, **454**, L85
 Dodonov S. N., Kotov S. S., Movsesyan T. A., Gevorgyan M., 2017, *Astrophysical Bulletin*, **72**, 473
 Doroshenko V. T., Sergeev S. G., Klimanov S. A., Pronik V. I., Efimov Y. S., 2012, *MNRAS*, **426**, 416
 Egorov O. V., Lozinskaya T. A., Moiseev A. V., Smirnov-Pinchukov G. V., 2018, *MNRAS*, **478**, 3386
 Eracleous M., Halpern J. P., 1993, *ApJ*, **409**, 584
 Fischer T. C., et al., 2017, *ApJ*, **834**, 30
 Freitas I. C., et al., 2018, *MNRAS*, **476**, 2760
 Kauffmann G., et al., 2003, *MNRAS*, **346**, 1055

Keel W. C., et al., 2012, *MNRAS*, **420**, 878
 Keel W. C., et al., 2015, *AJ*, **149**, 155
 Keel W. C., et al., 2017, *ApJ*, **835**, 256
 Kenney J. D. P., Tal T., Crowl H. H., Feldmeier J., Jacoby G. H., 2008, *ApJ*, **687**, L69
 Kewley L. J., Dopita M. A., Sutherland R. S., Heisler C. A., Trevena J., 2001, *ApJ*, **556**, 121
 Khachikian E. E., Weedman D. W., 1971, *Astrofizika*, **7**, 389
 Kharb P., O’Dea C. P., Baum S. A., Colbert E. J. M., Xu C., 2006, *ApJ*, **652**, 177
 Kharb P., O’Dea C. P., Baum S. A., Hardcastle M. J., Dicken D., Croston J. H., Mingo B., Noel-Storr J., 2014, *MNRAS*, **440**, 2976
 Kukula M. J., Holloway A. J., Pedlar A., Meaburn J., Lopez J. A., Axon D. J., Schilizzi R. T., Baum S. A., 1996, *MNRAS*, **280**, 1283
 Lintott C. J., et al., 2009, *MNRAS*, **399**, 129
 Magnier E. A., et al., 2016, preprint, ([arXiv:1612.05242](https://arxiv.org/abs/1612.05242))
 Mapelli M., Moore B., Bland-Hawthorn J., 2008, *MNRAS*, **388**, 697
 Meaburn J., Whitehead M. J., Pedlar A., 1989, *MNRAS*, **241**, 1P
 Mingo B., Hardcastle M. J., Croston J. H., Evans D. A., Hota A., Kharb P., Kraft R. P., 2011, *ApJ*, **731**, 21
 Moiseev A. V., 2014, *Astrophysical Bulletin*, **69**, 1
 Morganti R., 2017, *Nature Astronomy*, **1**, 596
 Osterbrock D. E., Koski A. T., 1976, *MNRAS*, **176**, 61P
 Reshetnikov V., Sotnikova N., 1997, *A&A*, **325**, 933
 Schawinski K., Thomas D., Sarzi M., Maraston C., Kaviraj S., Joo S.-J., Yi S. K., Silk J., 2007, *MNRAS*, **382**, 1415
 Smirnova A., Moiseev A., 2010, *MNRAS*, **401**, 307
 Yoshida M., et al., 2004, *AJ*, **127**, 90